Catalysis Today xxx (xxxx) xxx

Contents lists available at ScienceDirect

Catalysis Today

journal homepage: www.elsevier.com/locate/cattod

Multicomponent graphene based catalysts for guaiacol upgrading in hydrothermal conditions: Exploring "H_2-free" alternatives for bio-compounds hydrodeoxygenation

Silvia Parrilla-Lahoz [a,c], W. Jin [b], L. Pastor-Pérez [c], M.S. Duyar [a], Laura Martínez-Quintana [a], A.B. Dongil [b], Tomas Ramirez Reina [a,c,*]

[a] Department of Chemical and Process Engineering, University of Surrey, Guildford GU2 7XH, UK
[b] Institute of Catalysis and Petrochemistry, ICP-CSIC, Madrid, Spain
[c] Inorganic Chemistry Department & Material Science Institute, University of Seville-CSIC, Avda. Américo Vespucio 49, Sevilla 41092, Spain

ARTICLE INFO

Keywords:
H2-free HDO
Guaiacol
Biomass
Zr
Ni
Gr
N-doped catalysts

ABSTRACT

Catalytic hydrodeoxygenation (HDO) is a critical technique for upgrading biomass derivatives to deoxygenated fuels or other high-value compounds. Phenol, guaiacol, anisole, p-cresol, m-cresol and vanillin are all monomeric phenolics produced from lignin. Guaiacol is often utilised as a model lignin compound to deduce mechanistic information about the bio-oil upgrading process. Typically, a source of H_2 is supplied as reactant for the HDO reaction. However, the H_2 supply, due to the high cost of production and additional safety precautions needed for storage and transportation, imposes significant economic infeasibilities on the HDO process's scaling up. We investigated a novel H_2-free hydrodeoxygenation (HDO) reaction of guaiacol at low temperatures and pressures, using water as both a reaction medium and hydrogen source. A variety of Ni catalysts supported on zirconia/graphene/with/without nitrogen doping were synthesised and evaluated at 250 °C and 300 °C in a batch reactor, with the goal of performing a multi-step tandem reaction including water splitting followed by HDO. The catalysts were characterised using H_2-TPR, XRD, TEM and XPS to better understand the physicochemical properties and their correlation with catalytic performance of the samples in the HDO process. Indeed, our $NiZr_2O$/Gr-n present the best activity/selectivity balance and it is deemed as a promising catalyst to conduct the H_2-free HDO reaction. The catalyst reached commendable conversion levels and selectivity to mono-oxygenated compounds considering the very challenging reaction conditions. This innovative HDO approach provides a new avenue for cost-effective biomass upgrading.

1. Introduction

Within the renewable energy portfolio, biomass is a key resource for mitigating climate change and reducing reliance on fossil fuels [1]. Lignin is a major component of biomass and has the potential to be converted into hydrocarbon fuels and value-added compounds [1]. Fast pyrolysis technique may be used to extract desired compounds from biomass, and the liquid produced is referred to as bio-oil [1]. Bio-oils produced from the rapid pyrolysis of lignin often include a high concentration of oxygenated compounds. Due to the high oxygen content of bio-oil, it has significant disadvantages such as high viscosity, low solubility in other hydrocarbons, low volatility, corrosiveness, and low heating value, which prevents its direct use as a transportation fuel [2]. Additionally, the reactive compounds have extremely low stability during the storage process. As a result, in order to create carbon neutral fuels from bio-oil, it must be upgraded to meet these fuel specifications.

Catalytic hydrodeoxygenation (HDO) is one of the rapidly developing technologies for upgrading bio-oils to produce transportation fuel or value-added chemicals [1]. This process is generally performed by using a hydrotreating process under high pressure [3]. It is essential to deoxygenate bio-oils to eliminate the high viscosity and chemical instability and also increase heating value [2]. Ideally, oxygen is removed in the presence of catalyst with minimal saturation of the aromatic rings, which also reduces the hydrogen consumption [1].

In order to make the HDO process more economically appealing, H donors other than hydrogen gas have been considered as alternatives

* Correspondence to: Department of Chemical and Process Engineering, University of Surrey, Guildford GU2 7XH, UK.
E-mail address: t.ramirezreina@surrey.ac.uk (T.R. Reina).

https://doi.org/10.1016/j.cattod.2023.01.027
Received 2 November 2022; Received in revised form 13 January 2023; Accepted 26 January 2023
Available online 27 January 2023

[4]. Water is a cheap and available source of hydrogen that near its critical point can also be an excellent solvent for liquid phase HDO, making the process sustainable and economically more feasible. In this alternative process, catalysts must be designed to facilitate water dissociation on the surface, which will provide hydrogen to the catalytic HDO reaction. Noble metal and non-noble metal catalyst supported on carbon have been studied by our research group before, demonstrating the feasibility of the viability of "H2-free" HDO reactions using water as reaction media [4–7]. Generally speaking, noble metals present higher activity compared to transition metal catalysts. Ru/C displays the highest activity among studied catalysts (i.e. Au/C, Pd/C, Rh/C and Ru/C). The high activity is attributed to the smaller mental particle size, greater dispersion of metal particles and its intrinsic activity for this reaction [4].

Guaiacol has been selected as lignin model compound for the HDO reaction because the molecule is composed of two typical functional groups, i.e. hydroxy and methoxy groups [2]. The targeted products of guaiacol HDO reaction are ideally hydrocarbons or hydrogenated aromatic compounds. Transition metal-based catalysts, noble metal catalysts and zeolites-based catalysts have been widely investigated to produce hydrodeoxygenated aromatic compounds from guaiacol. To assist HDO reactions two functions are required for the catalyst, including the activation of the oxygen containing groups on the reactant (water activation) and the hydrogen donation (hydrodeoxygenation reaction) [4,6,7]. For noble metal catalysts such as Pd/C, Rh/C, Au/C, Ru/C and Pt/NC [4,6,7], the activation of the O-containing groups on the reactant take place on the metal sites or the metal-support- interface, and the hydrodeoxygenation reaction occurs on the surface of noble metals [1]. Despite their high activity and stability in the HDO reaction, noble metals constitute critical raw materials with limited availability, and it is necessary to identify earth abundant, low-cost alternatives which are more sustainable. Ni catalysts have been extensively investigated in HDO process considering the cheap price and similar performance in comparison to the noble metal catalysts [8]. Ni-based catalysts have good capability towards C-C bond rupture, and high activity in hydrogenation. However, Ni catalysts are susceptible to coke deposition, leading to the deactivation of the catalyst and hence poor stability [5]. The selection of support can significantly influence coking resistance of Ni-based catalysts [9]. It is reported that the performance of the conventional catalysts can be improved by using Zr_2O as promoter in order to prevent coke deposition [10]. Therefore, Zr_2O was explored as a promoter for this research effort.

Carbon materials are ideal candidates for catalysts supports for HDO reaction, since they are inert, with limited interactions with the active phase. Activated carbon is also a viable support considering its hydrophobicity, which could decrease the possibility of metal deactivation in water-existing reaction systems [11]. Graphene and its derivates deserve more attention due to their large surface area, and unusual electronic, mechanical, and thermal properties [12]. Graphene consists of a monolayer of carbon atoms arranged in a hexagonal structure. It is reported that graphene supported catalysts present the highest activity in deoxygenation of vegetable oil among other carbon materials including glassy spherical carbon, activated carbon and mesoporous carbon. The superior activity can be attributed to its large pore size, which facilitates the transportation of reactant and fine dispersion of metal particles on the surface of graphene support [12]. To optimise metal-graphene interaction, further actions could be done such as reducing the nanoparticle sizes, improving the homogeneous distributions of the nanoparticles and increasing the number of defect sites on graphene surfaces [13]. Various methods have been proposed to engineer the electronic structure of graphene, including preparing carbon sheets with different layers and graphene with and without defects, chemical functionalities of graphene, and chemical doping [14,15]. Chemical doping is the introduction of a heteroatom substituting a carbon atom in the graphitic structure [16]. Nitrogen substitution are considered magnificent candidates owing to the fact that they have comparable atomic size and strong valence bonds with carbon atoms [15,16]. The increased deoxygenation capacity of the N-doped samples is attributed to increased activity of the N-support and N-metal interfaces. Such interfaces are envisioned as electron-rich regions capable of activating C-O bonds [17].

In our work, different Ni-based graphene supported catalysts with/without nitrogen doping have been synthesised, characterised, and studied in guaiacol HDO reaction using water as hydrogen supplier. Consequently, in this study, the effect of synthesis methods, nitrogen doping and the addition of ZrO_2 as a promoter were explored.

2. Materials and methods

2.1. Supports

Reduced graphene oxide (Gr) and N-doped reduced graphene oxide (Gr-n) were employed as supports in this investigation. As a precursor, graphite oxide (GO_{325}) was required for the production of both Gr and Gr-n. GO_{325} was made using commercial natural flake graphite (G, 99.9% purity) obtained from Alfa Aesar and a modified Brodie process [18]. The reduced graphene oxides were created by thermally reducing GO_{325} in a vertical cylindrical packed bed reactor. The reactor was loaded (350 mg GO_{325}) and purged with N_2 for one hour at room temperature at a flow rate of 100 sccm. Following that, the N_2 flow was lowered to 87 sccm, and a flow of 3 and 10 sccm H_2 and NH_3 respectively, were introduced into the reactor for the N-doped sample. Then, several temperature treatment programs were used. The initial ramp was from room temperature to 100 °C at a rate of 5 °C/min. After that, it was raised to 700 °C at a rate of 5 °C/min and held at that temperature for 5 min. After the furnace heating was completed, the reactor was allowed to cool to 400 °C, the H_2/NH_3 flows were turned off, and the system was allowed to cool in N_2 atmosphere. This graphene was given the name Gr-n. The reduction of the undoped sample was carried out in the same manner as stated above, but without the addition of NH_3 to the reactor; this graphene was designated as Gr.

2.2. Catalyst preparation

Four types of catalysts, labelled as Ni/Gr, Ni/Gr-n, $NiZrO_2$/Gr and $NiZrO_2$/Gr-n were synthesised.

Wet impregnation synthesis method it is utilised for supported catalysts. Firstly, the necessary amounts of metal precursor ($Ni(NO_3)_2{\cdot}6H_2O$) were dissolved in deionised water and added to the support that was prior synthesised. After that, in order to obtain homogeneity of the suspensions, they were stirred at room temperature. Secondly, the excess water was removed in a rotary evaporator under reduced pressure and the materials were dried in an oven at 80 °C for 12 h. The last step of the method was the calcination at 500 °C (5 °C/min ramp) for 3 h under an inert atmosphere.

10 wt% ZrO_2 was impregnated on Gr and Gr-n. 0.0989 g $Zr(NO)_36H_2O$ was dissolved in 50 mL of acetone, and 350 mg of the appropriate support was added while stirring for 4 h. The solvent was then evaporated, and the resultant sample was dried in an oven at 100 °C overnight. The samples were then calcined at 350 °C for 5 h with a temperature ramp of 1 °C/min. Then, by using $Ni(NO_3)_2{\cdot}6H_2O$ as a precursor salt and the same process as described above, impregnation of 15 wt% Ni was carried out. Ni loading was the same for all synthesized catalysts. Sigma-Aldrich supplied all of the reactants.

2.3. Catalyst characterisation

The catalysts have been characterised by means of XRD, H_2-TPR, TEM and XPS.

XRD. X-ray diffraction (XRD) analysis was conducted on fresh, reduced and used catalysts using an X′Pert Pro Powder Diffractometer by PANalytical. The 2θ angle was increased by 0.05° every 240 s over

the range of 10–80 °. Diffraction patterns were recorded at 40 mA and 45 kV, using Cu Kα radiation (λ = 0.154 nm).

H_2-TPR. Temperature programmed reduction with hydrogen (TPR) analysis was carried out on the calcined catalysts in a quartz tube reactor. 50 mg of sample was heated to 900 °C at a rate of 10 °C/min with a total flow of 50 mL min^{-1} of 5% H_2 in N_2. A CO_2-ethanol trap was used to condense the gaseous products, mostly water, before the on-stream thermal conductivity detector (TCD). The H_2 uptake was quantified by comparison with the hydrogen consumption of a CuO reference sample.

TEM. Information about the supported metal particles was acquired by TEM (Transmission electron microscopy) in a JEOL 2100 F field emission gun electron microscope operated at 200 kV and equipped with an Energy-Dispersive X-Ray detector, XEDS. The sample was ground until powder and a small amount was suspended in acetone solution using an ultrasonic bath. Some drops were added to the copper grid (Aname, Lacey carbon 200 mesh) and the solvent was evaporated at room temperature before introduction in the microscope. XEDS-mapping analysis was performed in STEM mode with a probe size of 1 nm using the INCA x-sight (Oxford Instruments) detector.

XPS. The XPS spectra were obtained by using non-monochromatic Al radiation (200 W, 1486,61 eV) through a SPECS GmbH with UHV system and with an energy analyser (PHOIBOS 150 9MCD). The samples were pre-treated at 500ºC for an hour in H2 and subsequently, for another hour in He at room temperature. After that, the samples were placed in the sample holder using a double-sided copper tape and transferred to the analysis chamber. The survey spectra were obtained with a 50-eV pass energy and region spectra were obtained at 20 eV pass energy. The binding energy (BE) was finally measured taking as a reference the C1s peak at 284.6 eV and the equipment error was considered as less than 0.01 eV for the determination of energies.

2.4. Catalytic reactions

The HDO reactions were conducted in a batch reactor (Parr Series 5500 HPCL Reactor with a 4848 Reactor Controller) using 300 mL PTFE gaskets. Catalysts were pre-treated ex-situ in a continuous flow quartz reactor, at 550 °C for 1 h in a 100 mL/min gas flow (H_2:Ar=1:4) before being used in the HDO reaction. A quantity of 0.5 g of guaiacol, 49.5 g of water and 0.05 g of catalyst were loaded in a glass-lined steel vessel. To avoid any air contamination, N_2 was bubbled through the solution for 5 min under a stirring speed of 100 rpm before closing the reaction vessel. Then, the reactor was heated to the desired temperature (250 °C/300 °C) and held at this temperature for 4 h under a stirring speed of 300 rpm. The pressure of the vessel was fixed according to the natural pressure generated by the solvent (water) at 50/100 bar during the reactions respectively. After the reaction, the spent catalyst was recovered from the liquid by filtration, followed by drying treatment. The organic products were dissolved and recovered with ethyl acetate extraction. The organic compounds products were identified by a gas chromatography-mass spectrometry (GC-MS). Quantitative analysis was performed with a gas chromatograph-flame ionisation detector (GC/FID). The GC injector temperature was 280 °C. The GC separation was performed by using a Carboxen Packed Analytical Column (30 m×320 μm×0.25 μm). A split ratio of 8:1 was held. The column was firstly held at 50 °C for 1 min, then increased to 240 °C at a heating rate of 5 °C/min and held at 240 °C for 10 min

The conversion of guaiacol and selectivity (based on C mol) of the products was calculated using Equation 1 and 2, respectively.

$$\textit{Conversion of Guaiacol}\left(\textit{mol}\ \%\right) = \frac{\frac{(m_{Gin}-m_{Gout})*N_G}{M_G}}{m_{Gin}/M_G * N_G} * 100 \quad (1)$$

$$\textit{Carbon weighted selectivity of product x}\left(\textit{mol}\ \%\right) = \frac{\frac{m_x*N_x}{M_x}}{\frac{(m_{Gin}-m_{Gout})*N_G}{M_G}} * 100 \quad (2)$$

m_{Gin}: Initial mass of guaiacol [gr]; m_{Gout}: Detected mass of guaiacol in the organic phase [gr]; m_x: Mass of product x [gr]. M_G: Molar mass of guaiacol[mol/gr]; M_x: Molar mass of product x[mol/gr]. N_G: Number of Carbon in guaiacol; N_x: Number of Carbon in product x.

3. Result and discussion

3.1. Catalytic activity

3.1.1. Catalytic behaviour of calcined catalyst

The catalytic behaviour of the reduced catalysts in the guaiacol HDO process was studied at 250 °C and 300 °C for 4 h. Activity results are displayed in Figs. 1 and 2. Numerical data can be found in the supporting information (Tables 1 and 2 respectively).

The reaction results of our Ni-based catalysts at 250 °C are presented in Fig. 1. Guaiacol conversion of all the catalysts varied between 15% and 20%. Such conversion ranges might look modest however we shall emphasise that in our study the HDO process is conducted using water as hydrogen source and suppressing completely external H_2 input our reaction system. Hence these are interesting results given the significant process savings. A clear effect of the N-doping on the catalytic activity was seen since the Ni/Gr-n exhibited the highest guaiacol conversion (20%) compared to 17% of the undoped catalyst. However, no promotion effect on the conversion of guaiacol was observed when ZrO_2 was added as a promoter.

Three mono-aromatic compounds including phenol, cresol and catechol were detected on the organic phase. Such products are associated with a potential guaiacol HDO reaction pathway proposed in Fig. 3. The formation of catechol is the most preferred process because the C(sp^3)-O bond is most likely to be broken owning to its low bond energy [19]. Despite retaining two oxygens, catechol is one of the intermediates that ultimately leads to more advanced (more deoxygenated) products such as phenol (1 oxygen), benzene, or cyclohexane (fully deoxygenated products) [5]. The production of partial deoxygenated compounds phenol and catechol were improved over Ni/Gr catalyst in comparison to all other samples indicating the superior ability of demethoxylation and/or dihydroxylation [5]. When N was present, the results showed slight variations between the catalysts. The N-doped catalysts produced some phenol, showing that the C-O cleavage was preferred in N-doped systems. The latter is consistent with previous studies of palm oil HDO utilising N-doped activated carbons catalysts, in

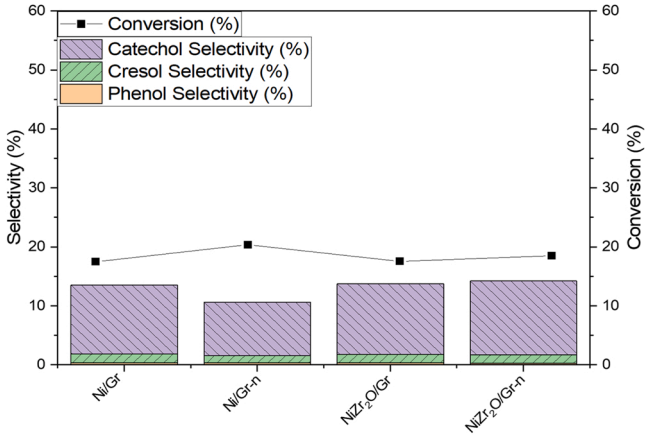

Fig. 1. H_2-free HDO of guaiacol at 250 °C and 50 bar during 4 h for all samples.

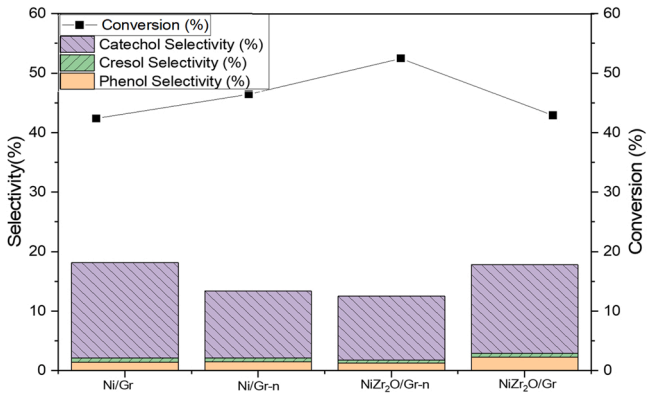

Fig. 2. H_2-free HDO of guaiacol at 300 °C and 100 bar during 4 h for all samples.

Table 1
Data of the N1s region XPS.

Catalyst	N 1 s (eV, at%)			
	N1s pyr	N1s pyrr	N 1 s quater	N 1 s $_{NOx}$
$NiZr_2O$/Gr-n PR	398.3 (36.1)	399.7 (25.7)	401.0 (25.1)	403.7 (13.1)
Ni/Gr-n	398.1 (35.9)	399.4 (25.4)	401.0 (26.3)	404.5 (12.4)
$NiZr_2O$/Gr-n	398.1 (36.7)	399.0 (26.9)	400.8 (25.0)	404.1 (11.4)

Table 2
binding energies (B.E), atomic percentages and relative proportions.

		Ni 2p 3/2 (eV, at%)			
Catalyst	Ni sat	Ni sat	Ni 2 +	Ni 2 +	Ni (0)
Ni/Gr PR	866.7	863.5	860.7	857.4	
	(21.1)	(12.5)	(43.5)	(22.9)	
$NiZr_2O$/Gr	866.0	862.6	860.3	857.3	
PR	(24.9)	(19.3)	(24.9)	(32.9)	
$NiZr_2O$/Gr-n	865.0	861.4	859.2	854.8	
PR	(21.2)	(9.0)	(43.7)	(26.1)	
Ni/Gr	861.2		858.1	855.3	852.8
	(15.2)		(3.1)	(49.9)	(26.2)
Ni/Gr-n	861.2		857.7	855.4	853.0
	(21.4)		(8.8)	(29.8)	(40.0)
$NiZr_2O$/Gr	861.8		858.5	855.4	852.8
	(12.7)		(14.6)	(47.0)	(25.7)
$NiZr_2O$/Gr-n	860.8			855.2	853.0
	(10.7)			(34.3)	(55.1)

which the increased deoxygenation capacity of the N-doped samples is attributed to increased activity of the N-support and N-metal interfaces. Such interfaces are envisioned as electron-rich regions capable of activating C-O bonds [17]. Overall, all three samples have similar selectivity towards phenol, cresol and catechol being phenol the most advanced deoxygenation product since it represents just the last step prior to benzene, the final product in the deoxygenation route according as depicted in Fig. 3. Indeed phenol presence in our liquid products mixtures is an encouraging results since despite the absence of external hydrogen source our catalysts can trigger the reaction and get very close to full deoxygenation.

To enhance conversion levels, the reaction temperature was raised to 300 °C. Catalytic behaviour of Ni-based catalysts and Gr-supports at 300 °C are presented in Fig. 2, where differences in activity can be observed. Guaiacol conversion of all the catalysts varied between 40% and 55%. This guaiacol conversion was almost doubled in comparison with the catalytic activity presented at 250 °C in Fig. 1 showcasing that upon tunning the reaction parameters remarkable catalytic performance boosting can be attained. Although a full reaction parameters optimisation is beyond the scope of this proof-of-concept paper this result suggests there is big room for overall process improvement reinforcing the potential of "H_2-free" HDO strategies.

The conversion increased at 300 °C compared to that obtained at 250 °C is a general trend for all the studied catalysts. For example, the conversion of guaiacol obtained over calcined Ni/Gr (17%) at 250 °C was 26% lower compared to that obtained over reduced Ni/Gr (43%) catalyst at 300 °C. Also, temperature and pressure had a greatest influence on the activity of Ni-Gr sample, since 20% of guaiacol conversion was obtained at 250 °C and 45% of guaiacol conversion at 300 °C. By comparing both Figs. (1 and 2), we can determine that temperature and pressure had great influence on the catalytic performance. Therefore, we can conclude that during the HDO process an increase of 50 °C in temperature improved notably the conversion of guaiacol. More remarkably, both the addition of the catalyst and the rise of temperature and pressure, had a positive effect on the selectivity of the products and conversion of the guaiacol. Furthermore, promotion effect on the conversion of guaiacol was observed when adding ZrO_2 as a promoter at 300 °C, due to the enhanced oxygen mobility provided by ZrO_2 which allowed the activation of C-O bonds [10]. The presence of nitrogen modifies the electrical density and acid/base characteristics of carbon, hence influencing its overall reactivity. As previously reported by W. Jin and co-workers, the increased activity of N-doped supports is due to the beneficial effect of nitrogen, which might aid to stabilize metal particles and prevent their re-oxidation [17]. In addition, nitrogen sites inserted into the carbon network are envisioned as electron-rich reaction sites. Regardless of the reaction routes, there is no question that N as a dopant has a favourable influence on the upgrading reaction [17]. To conclude, the $NiZr_2O$/Gr-n catalyst showed the best result according to the objective, since the production of cresol has been enhanced as a reaction product and is the catalyst that shows best catalytic activity. By nitrogen-doping our carbon support, we may possibly increase the activity [17]. In view of these results, Ni-based catalysts are also an advisable choice considering their relatively low price.

It is pointed out that the products analysed were the dominant products in the organic liquid phase. The rest of compounds, up to 100% of selectivity were other aromatics hydrocarbons in addition to some secondaries products derivates of reactions like decarboxylation cracking, and hydrocracking can be found. In terms of selectivity results, three partially deoxygenated mono-aromatic compounds, namely phenol, cresol and catechol were detected in the organic phase as per observed also at 250 °C. The production of the partial deoxygenated products phenol and cresol was improved over Ni/Gr catalyst, indicating its superior ability of demethoxylation and/or dihydroxylation at 300 °C.

A schematic representation of the potential HDO pathways of guaiacol is proposed in Fig. 3 [20]. The high selectivity of catechol in all the product distribution indicated a preferential HDO pathway. The formation of catechol was the most preferred process because the C (sp3)- O bond was most likely to be broken, since it presented the lowest bond energy [19]. Unfortunately, benzene was not produced in our reaction system. This result should not be considered unfavourable since the main challenge in an "H_2-free" HDO process is to incorporate the hydrogen into the organic molecules without an external H_2 supplier. It is important to remember that because we are engaging in an HDO process in which there is no addition of external hydrogen, only locally produced hydrogen during the reaction may combine with the oxygenated molecules. However, the process economic viability and safety issues attributed to hydrogen manipulation and transport make this pathway desirable for oxygenated hydrocarbon upgrading despite the generally low conversion values reported.

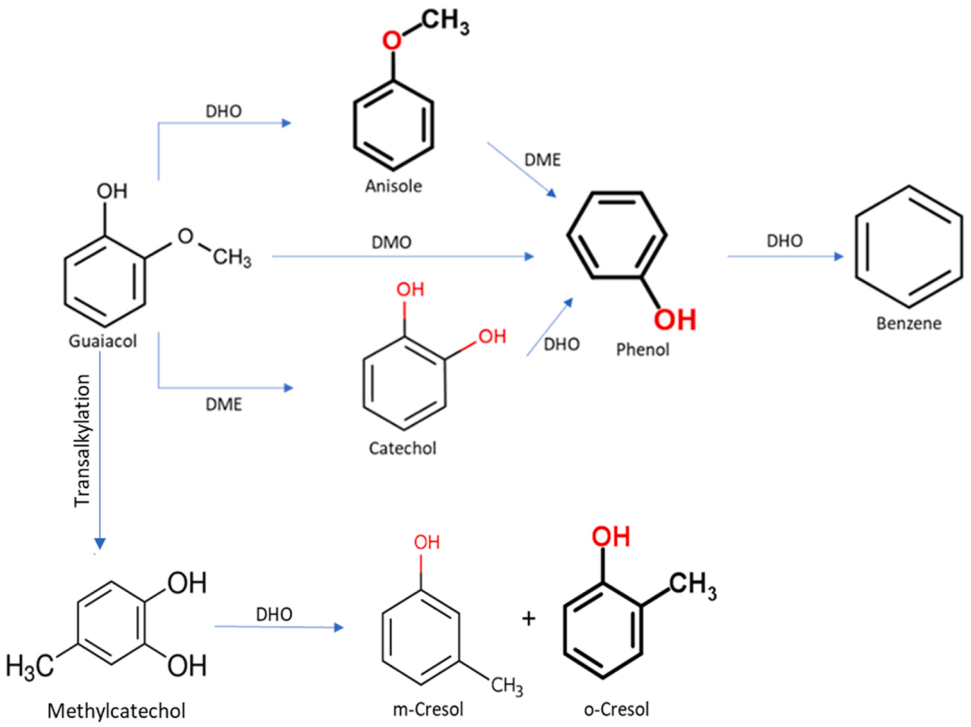

Fig. 3. Proposed reaction pathways of guaiacol HDO over noble metal catalysts (DMO: Demethoxylation DME: Demethylation; DHO: Dehydroxylation) [20].

3.2. Characterization

3.2.1. Characterization of fresh samples

3.2.1.1. XPS. A quantitative analysis of the nitrogen species presents in the samples was obtained by deconvolution of the XPS spectra of the N1s core level. In Table 1, the data of the N1s region XPS analyses are shown for selected catalysts. The main nitrogen component on the fresh and reduced catalyst is pyridinic nitrogen followed by pyrrolic and quaternary which have been created with similar ratio. The similar ratios and binding energies obtained on both the fresh and spent catalysts seem to indicate that the nitrogen species are stable under reaction conditions.

The XPS spectra of Ni $2p_{3/2}$ in the reduced-passivated catalyst is shown in Fig. 4. The corresponding binding energies (B.E), atomic percentages and relative proportions are provided in Table 2. Ni/Gr and, $NiZr_2O$/Gr catalysts exhibited a peak at 852.8 eV and NiGr -n showed a peak at 853.0 eV, corresponding these peaks to Ni^0. In these catalysts, peaks at higher B.E associated to Ni^{2+} are also observed. Ni/Gr catalyst could be deconvoluted into contributions at 861.2 eV (Ni^{2+} satellite peak), 858.1 eV and 855.3 eV (Ni^{2+}) and 852.8 eV (Ni^0). $NiZr_2O$/Gr, Ni/Gr-n and $NiZr_2O$/Gr-n exhibited similar species. This suggests the presence of metallic Ni and Ni^{2+} species on the support's surface of the catalysts, in accordance with the XRD data obtained (Fig. 5). In Table 2 it is observed that the atomic percentages of Ni^0 are higher in the Ni/Gr-n and $NiZr_2O$/Gr-n catalyst than in the Ni/Gr and $NiZr_2O$/Gr catalyst, suggesting a possible stabilising effect of nitrogen on the metallic Ni in good agreement with the H_2-TPR data described below.

3.2.1.2. XRD. Fig. 5 shows the different XRD pattern of Ni/Gr, Ni/Gr-n, $NiZr_2O$/Gr and $NiZr_2O$/Gr-n samples for fresh, reduced and post reaction (at 250 °C and 300 °C) catalyst forms.

A weak and broad diffraction peak at around $2\theta = 26.5°$ can be observed in the XRD patterns of Ni/Gr and $NiZrO_2$/Gr catalysts (Fig. 5 (A) and (C) respectively), assigned to the (002) planes of the graphitic carbon frame (JCPDS 41–1487) [21,22] with more amorphous structure and lower order in crystallinity. In contrast, this peak for n-doped samples was stronger and sharper, indicating a higher order of graphic structure. Moreover, these materials recovered the graphitic structure to a higher extent [23]. A second diffraction peak at 44.0° corresponding (100) plane of graphite indicated the reduction of the GO matrix [24,25]. However, this peak overlapped with the Ni metallic peak at $2\theta = 44.5°$ (JCPDS 87–0712).

An interesting finding was that metallic Ni (JCPDS 87–0712) [5] was the main phase instead of NiO for fresh catalysts (except Ni/Gr-n), but NiO presence could not be discarded as the main peak could overlapped with the Ni metallic peak. This was probably due to the partial reduction of NiO during calcination process assisted by the support [26]. No diffraction peak of NiO (JCPS 04–0835) appeared in the XRD patterns of all reduced samples, indicating the success of reduction pre-treatment. Moreover, NiO reduction zones have been observed in the TPR profiles, which are discussed below.

The characteristic diffraction peaks at $2\theta = 30.2°$, 34.5° and 50.2° corresponding to the (101), (110) and (200) refection of ZrO_2 phase (JCPDS 70–1769) [27,28] can be clearly observed in the XRD patterns of ZrO_2 containing catalysts (Fig. 5 C) and D)). The diffraction peaks of tetragonal phase of ZrO_2 were stronger and sharper in n-doped catalyst compared to that of non-doped sample. Results indicated that there was a higher extent of crystallinity of ZrO_2 in n-doped catalyst. However, the characteristic peaks of monoclinic phase ZrO_2 were not observed in our case. It is reported that the t-ZrO_2 phase is formed at 400 °C, since the synthesis temperature utilised was below this temperature mixed phase ZrO_2 (both t-ZrO_2 and m-ZrO_2) were not expected consistently with the XRD data [29].

3.2.1.3. H_2-TPR. Redox properties and information concerning metal-support interactions were studied by H_2-temperature-programmed-reduction (TPR) analysis. The H_2-TPR profile of Ni/Gr catalyst is shown in Fig. 6. Three reduction zones can be observed, at around 280 °C, 330 °C and 530 °C. They all corresponded to the reduction of finely dispersed NiO on the support. Normally, smaller particle size presents reduction zone at lower temperatures [30].

In case of Ni/Gr-n, it is hypothesised that when the Ni atom is placed onto the doped support, there is a repulsion between the Ni and the nitrogen dopant, causing the Ni atom to establish an association [14].

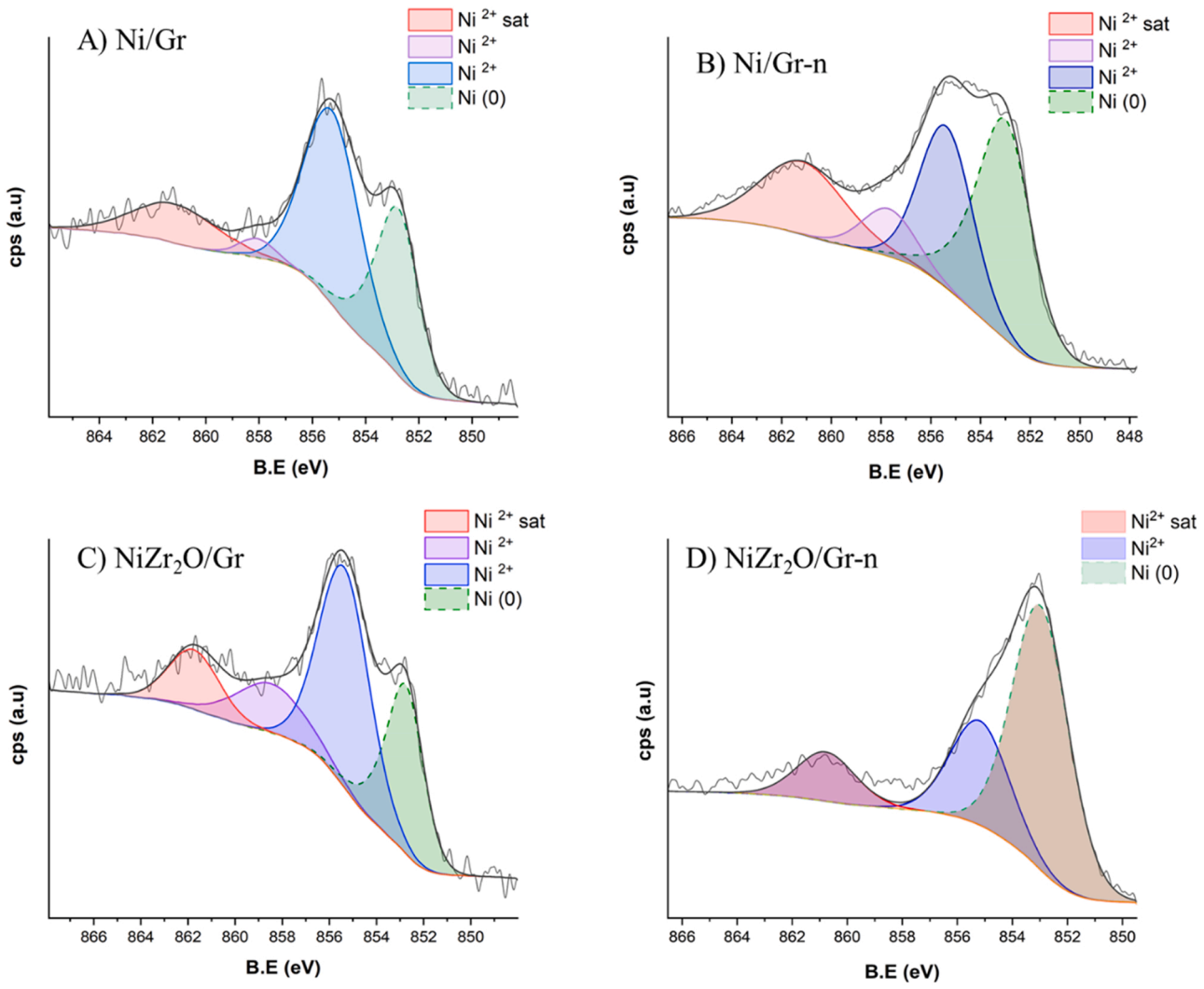

Fig. 4. The XPS spectra of Ni 2p3/2 in the reduced-passivated catalyst.

The dopant alters the local surface binding configuration, increasing the binding energy, and hence altering the Ni-carbon interaction. This implies that doping might boost the catalyst's durability [14].

In the $NiZrO_2$/Gr sample TPR profile, two reduction regions can be observed at 200 °C-400 °C and 550 °C-850 °C. The first peak centred at 250 °C is formed as a consequence of the NiO reduction on the support [30]. $NiZr_2O$/Gr sample has a lower reduction temperature, indicating it is easier to reduce. This might be due to lower particle size of Ni compared to the other samples due to the lower reduction temperatures in the TPR.The second peak was attributed to the reduction of oxygen superficial groups on the support [30]. In general, this peak is formed due to the reduction of finely dispersed NiO on the support, as when ZrO_2 is used in Ni-based catalysts it stabilises the cubic structure at high temperatures and improves oxygen storage capacity [31]. Moreover, it is important to mention that hydrogenation of carbon atoms in graphite [32] was taken into consideration at temperatures higher than 800 °C, since methane production has been observed in this temperature range. Two reduction peaks were present in the H_2-TPR profile of $NiZrO_2$/Gr-n sample, one at around 300 °C and around 500 °C. They all corresponded to the reduction of finely dispersed NiO on the support [30].

As observed in the TPR profiles, the highest reduction temperature of the metal active phase of the catalyst was around 550 °C. Therefore, this was the temperature selected to reduce the catalyst prior to the reaction, since it has been demonstrated in previous publications that the reduction of the active phase of the samples improve the catalytic performance [14]. The success of the reduction prior to the reaction has been demonstrated by the XRD patterns above.

3.2.1.4. TEM. Transmission Electron Microscopy (TEM) was used to study the composition and distribution of the different elements in the synthesised reduced samples. The TEM images of fresh Ni/Gr, Ni/ZrO_2Gr and Ni/ZrO_2Gr-n are presented in Fig. 7. The micrographs clearly showed the exfoliated graphene layers along with zirconia and some nickel particles.

In general, a better metal dispersion in the N-doped sample can be observed in the TEM images, corroborating that the presence of nitrogen in the sample can help to obtain a better dispersion of active phases, as discussed in the TPR analysis. Some areas were further analyzed by the corresponding Fast-Fourier transform (FFT) pattern, and they are shown in Fig. 8 A) and B). In general, a relevant search on several zones of the material, showed that the undoped sample barely displayed zones where Ni and ZrO_2 were collocated. In contrast, the catalyst $NiZrO_2$-Gr-n did present this Ni-Zr interaction. Moreover, the analysis of the FFT pattern confirmed that ZrO_2 was mainly present in its tetragonal phase.

3.2.2. Spent samples characterisation

3.2.2.1. XRD. Coking and metal sintering of active phase may happen under liquid phase reactions with high pressure [9]. Hence, the XRD patterns of spent catalysts were analysed. As shown in Fig. 5 (A, B, and

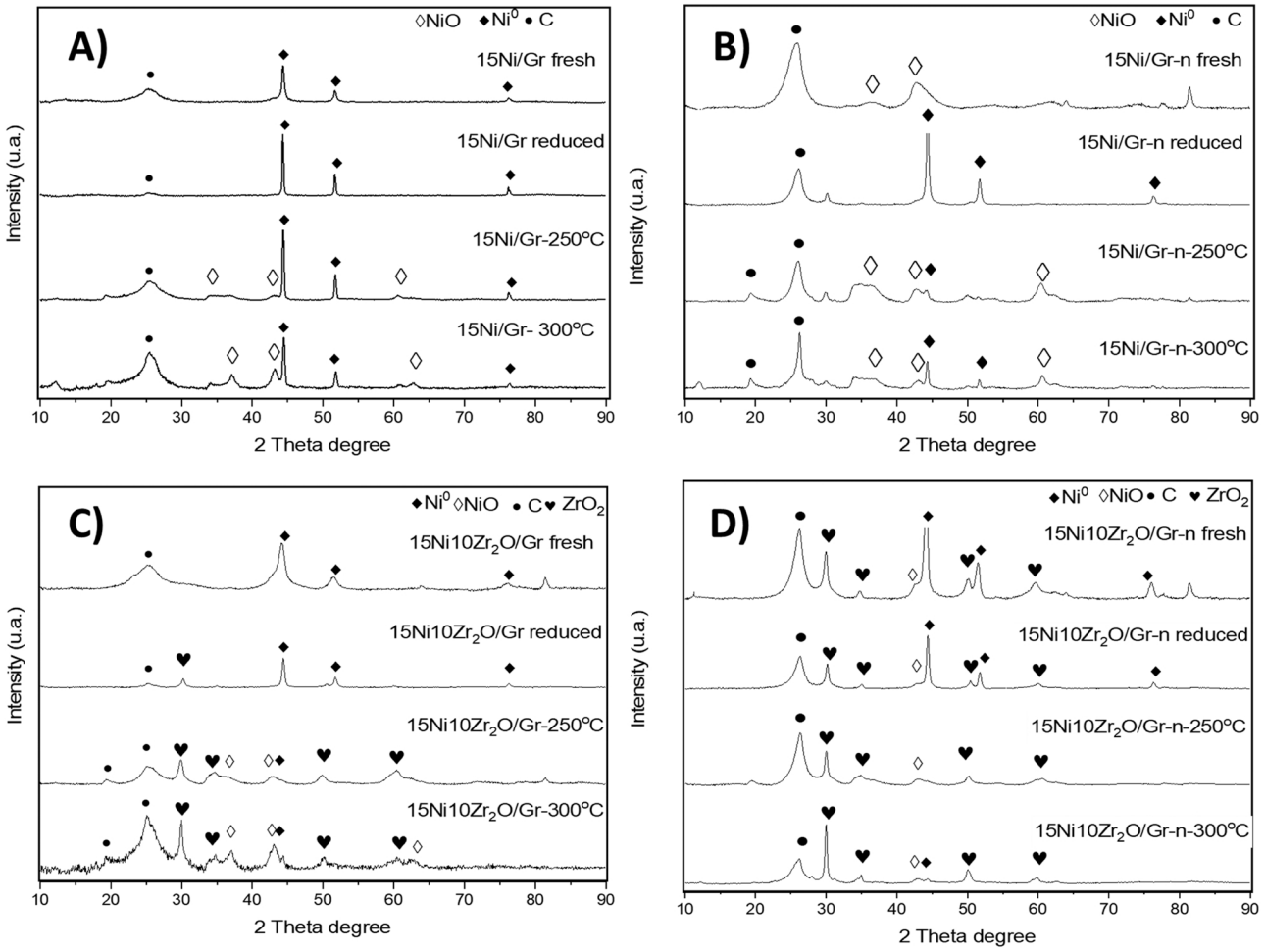

Fig. 5. XRD patterns of fresh, activated, and post-reactions (250 and 300 °C) Catalyst samples. A) Ni/Gr, B) Ni/Gr-n, C) NiZrO2/Gr and D) NiZrO2/Gr-n.

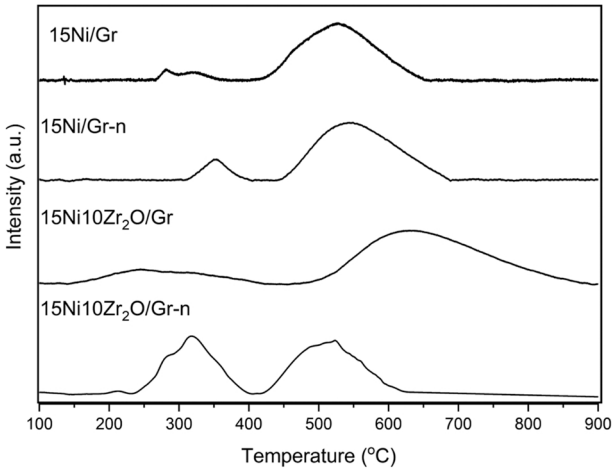

Fig. 6. H_2-TPR profiles of all calcined samples.

C), part or all of the metallic nickel were oxidized into NiO during the HDO reaction for Gr supported catalysts. In comparison to the calcined samples, some new diffractions peaks have been detected for the Ni/Gr, Ni/Gr-n, and $NiZrO_2$/Gr catalyst. Diffractions peaks at 37.3°, 43.3° and 63° were observed, corresponding to the (111), (200) and (220) planes of the NiO fcc phase respectively, in agreement with JCPDS no. 00–047–1049. This points out oxidation of the Ni metallic phase, which is partly expected given the selected reaction media (H_2O). On the other hand, such oxidation phenomenon was not observed for the $NiZrO_2$/Gr-n samples, hence reflecting higher stability due to the nitrogen doping and the ability of Zr to act as a promoter [10,16]. The different width of this peak is related to the different interlayer distance generated during the thermal reducing treatment. Therefore, it can be appreciated that at a higher the reaction temperature, the particle size increases and becomes more amorphous due to sintering of the metal phase.

3.2.2.2. TEM. TEM images of the samples (Ni/Gr, Ni/Gr-n, $NiZrO_2$/Gr and $NiZrO_2$/Gr-n) after the catalytic reaction at 300 °C are presented in Fig. 9. By comparing all figures, few particles agglomeration can be seen over $NiZrO_2$/Gr (Fig. 9 C)), but the particle distribution still remained homogenous for all samples. In comparison to the calcined samples, the sintering of the metal particles marginally increased the particle size. This was a result of the reduction procedure and reaction conditions used. Despite the very demanding reaction conditions, this finding demonstrated the structural and morphological stability of the $NiZrO_2$/Gr sample for the hydrothermal upgrading of lignin model compounds.

4. Conclusions

Based on a novel "H_2-free" HDO strategy, this research showcases a promising catalytic route for biomass upgrading. More specifically, we show that hydrothermal deoxygenation of guaiacol as a lignin model compound can be performed without external hydrogen input. For the in-situ production of hydrogen coupled to HDO, we propose multi-component catalysts capable of activating water and facilitating the

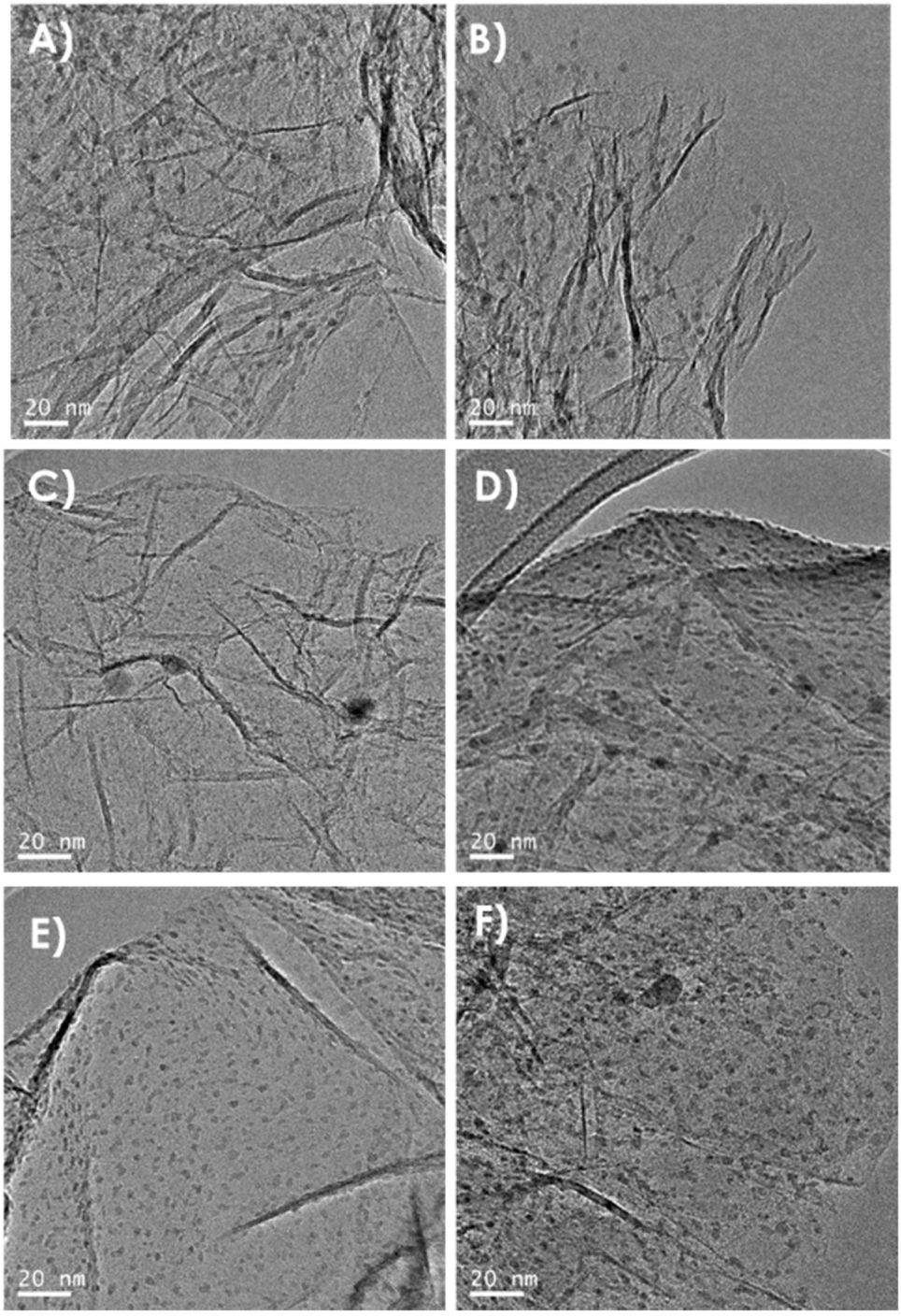

Fig. 7. TEM images A)B) Ni/Gr C)D)NiZr2O/Gr E)F)NiZr2O/Gr-n.

subsequent HDO reaction. Our catalysts based on Ni nanoparticles supported on N-doped and non-doped graphene decorated with zirconia particles were able to partially deoxygenate the original feedstock effectively. Furthermore, the samples were stable under the reaction conditions (high pressure, high temperature in a hydrothermal medium), as indicated by post-reaction XRD and TEM examination at 250 °C and 300 °C. Our results indicate that the $NiZr_2O$/Gr-n catalyst led to the best results, as the synthesis of cresol as a reaction product was increased, and it exhibited the highest catalytic activity. Cresol can be used as sources for high-value chemical products [33]. Nitrogen doping of the support was shown to improve conversion in all cases and is an effective strategy for promoting activity. In light of these findings, Ni-based catalysts are also a viable option for the HDO reaction of guaiacol due to their comparatively cheap cost and comparable catalytic performance compared to noble metal catalysts.

Overall, the catalytic performance of the designed catalysts may be considered moderate in contrast to existing catalysts in the standard HDO when high pressure hydrogen is supplied. Generally, it is necessary to increase overall deoxygenation efficiency by fine-tuning the catalyst composition for the water assisted HDO process. Also performing HDO of chemical intermediates (such as catechol) will aid to gather knowledge of the hydrogen transfer route and reaction pathways in the water assisted HDO process and further guide the catalysts design. Nonetheless, the distinctive benefit of our approach is the absence of external

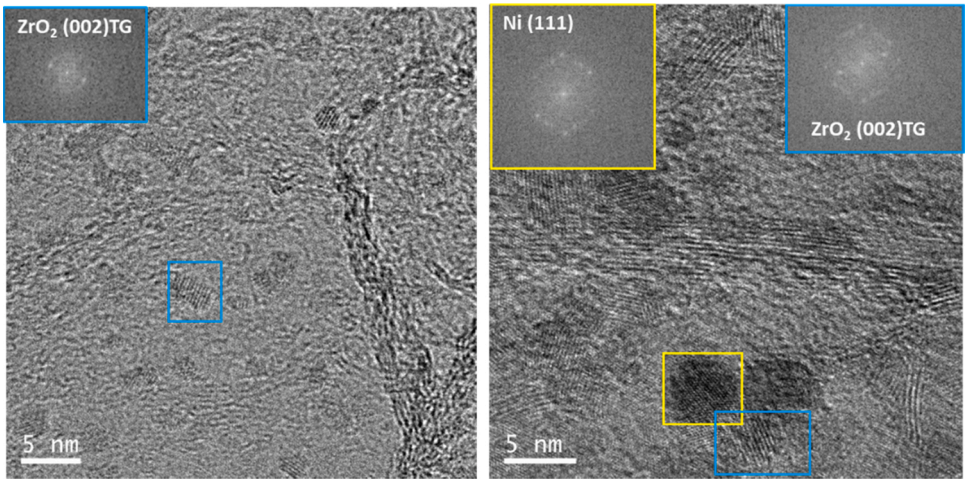

Fig. 8. A) TEM images NiZr2O/Gr. B) TEM images NiZr2O/Gr-n.

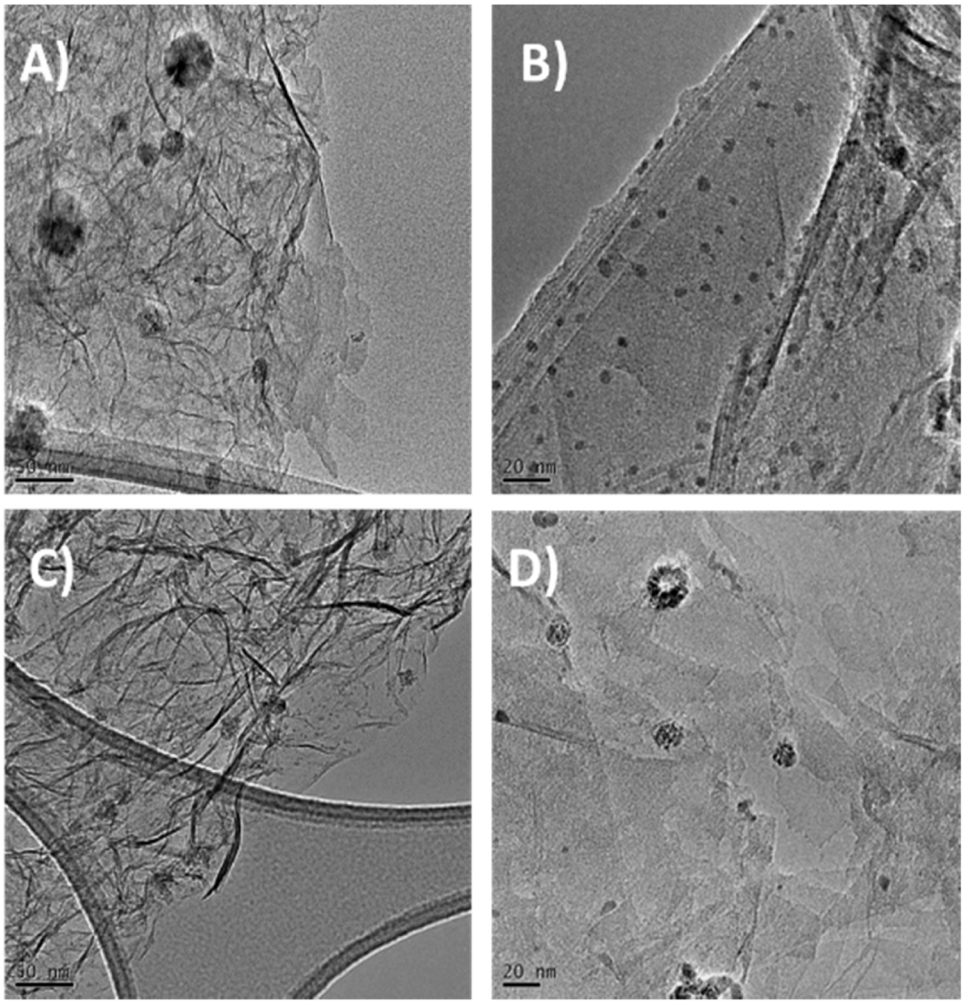

Fig. 9. TEM images of post reaction samples at 300 °C A)Ni/Gr, B) Ni/Gr-n, C)$NiZrO_2$/Gr and D)$NiZrO_2$/Gr-n.

hydrogen input. Hence, despite still on its early development stages, our concept should drive future research efforts to enhance the catalytic formulation and improve performance. In this approach, we demonstrate the crucial role of heterogeneous catalysis in bio-resources upgrading to aid in the transition to a low-carbon economy.

CRediT authorship contribution statement

S. Parrilla-Lahoz: Writing – original draft, Conceptualization, Visualization, Investigation. **W.Jin:** Writing – original draft, Conceptualization, Visualization, Investigation. **L. Pastor-Pérez:** Funding acquisition, Conceptualization, Project administration, Supervision. **M.S.**

Duyar: Funding acquisition, Conceptualization, Project administration, Supervision. **L.Martínez Quintana:** Experimental, Data curation. **A.B. Dongil:** Funding acquisition, Conceptualization, Project administration, Supervision. **T.R. Reina:** Funding acquisition, Conceptualization, Project administration, Supervision.

Declaration of Competing Interest

The authors declare that they have no known competing financial interests or personal relationships that could have appeared to influence the work reported in this paper: Tomas Ramirez Reina reports financial support was provided by Junta de Andalucía Consejería de Educación. Tomas Ramirez Reina reports financial support was provided by Spain Ministry of Science and Innovation.

Data Availability

Data will be made available on request.

Acknowledgements/Financial support

Financial support for this work has been obtained from Junta de Andalucía project P20-00667, co-funded by the European Union FEDER. This work is also sponsored by the Spanish Ministry of Science and Innovation through the projects PID2019-108502RJ-I00 and grant IJC2019- 040560-I both funded by MCIN/AEI/10.13039/501100011033 as well as RYC2018-024387-I funded by MCIN/AEI/10.13039/501100011033 and by ESF Investing in your future. Financial support from the European Commission through the H2020-MSCA-RISE-2020 BIOALL project (Grant Agreement: 101008058) and RYC2020-030626-I (MCIN) and project 20228AT002 (CSIC) is also acknowledged.

References

[1] D. Gao, C. Schweitzer, H.T. Hwang, A. Varma, Conversion of guaiacol on noble metal catalysts: reaction performance and deactivation studies, Ind. Eng. Chem. Res. 53 (2014) 18658–18667, https://doi.org/10.1021/ie500495z.

[2] Y.K. Hong, D.W. Lee, H.J. Eom, K.Y. Lee, The catalytic activity of Pd/WOx/γ-Al2O3 for hydrodeoxygenation of guaiacol, Appl. Catal. B Environ. (2014), https://doi.org/10.1016/j.apcatb.2013.12.045.

[3] J. Chang, T. Danuthai, S. Dewiyanti, C. Wang, A. Borgna, Hydrodeoxygenation of guaiacol over carbon-supported metal catalysts, ChemCatChem 5 (2013) 3041–3049, https://doi.org/10.1002/cctc.201300096.

[4] W. Jin, J.L. Santos, L. Pastor-Perez, S. Gu, M.A. Centeno, T.R. Reina, Noble metal supported on activated carbon for "Hydrogen Free" HDO reactions: exploring economically advantageous routes for biomass valorisation, ChemCatChem (2019) 4434–4441, https://doi.org/10.1002/cctc.201900841.

[5] W. Jin, L. Pastor-Pérez, J.J. Villora-Picó, A. Sepúlveda-Escribano, S. Gu, T.R. Reina, Investigating new routes for biomass upgrading: "h2-Free" hydrodeoxygenation using ni-based catalysts, ACS Sustain. Chem. Eng. (2019), https://doi.org/10.1021/acssuschemeng.9b02712.

[6] L. Pastor-pérez, W. Jin, J.J. Villora-picó, Q. Wang, M. Mercedes, A. Sepúlveda-escribano, T.R. Reina, "H2-free" demethoxylation of guaiacol in subcritical water using Pt supported on N-doped carbon catalysts: a cost-effective strategy for biomass upgrading, J. Energy Chem. (2020), https://doi.org/10.1016/j.jechem.2020.10.045.

[7] W. Jin, L. Pastor-Pérez, D.K. Shen, A. Sepúlveda-Escribano, S. Gu, T. Ramirez Reina, Catalytic upgrading of biomass model compounds: novel approaches and lessons learnt from traditional hydrodeoxygenation – a review, ChemCatChem 11 (2019) 924–960, https://doi.org/10.1002/cctc.201801722.

[8] L.C. Loc, P.H. Phuong, D. Putthea, N. Tri, N.T. Thuy Van, H.T. Cuong, Effect of CeO2 morphology on performance of NiO/CeO2 catalyst in combined steam and CO_2 reforming of CH4, Int. J. Nanotechnol. 15 (2018) 968–982, https://doi.org/10.1504/IJNT.2018.099935.

[9] W. Fang, C. Pirez, M. Capron, S. Paul, T. Raja, P.L. Dhepe, F. Dumeignil, L. Jalowiecki-Duhamel, Ce-Ni mixed oxide as efficient catalyst for H 2 production and nanofibrous carbon material from ethanol in the presence of water, RSC Adv. 2 (2012) 9626–9634, https://doi.org/10.1039/c2ra21701e.

[10] A. Gutierrez, R.K. Kaila, M.L. Honkela, R. Slioor, A.O.I. Krause, Hydrodeoxygenation of guaiacol on noble metal catalysts, Catal. Today (2009), https://doi.org/10.1016/j.cattod.2008.10.037.

[11] S. De, B. Saha, R. Luque, Hydrodeoxygenation processes: advances on catalytic transformations of biomass-derived platform chemicals into hydrocarbon fuels, Bioresour. Technol. 178 (2015) 108–118, https://doi.org/10.1016/j.biortech.2014.09.065.

[12] S.K. Kim, D. Yoon, S.C. Lee, J. Kim, Mo2C/graphene nanocomposite as a hydrodeoxygenation catalyst for the production of diesel range hydrocarbons, ACS Catal. 5 (2015) 3292–3303, https://doi.org/10.1021/acscatal.5b00335.

[13] Y. Wei, D. Luo, C. Zhang, J. Liu, Y. He, X. Wen, Y. Yang, Y. Li, Precursor controlled synthesis of graphene oxide supported iron catalysts for Fischer-Tropsch synthesis, Catal. Sci. Technol. 8 (2018) 2883–2893, https://doi.org/10.1039/c8cy00617b.

[14] S. Parrilla-Lahoz, W. Jin, L. Pastor-Pérez, D. Carrales-Alvarado, J.A. Odriozola, A. B. Dongil, T.R. Reina, Guaiacol hydrodeoxygenation in hydrothermal conditions using N-doped reduced graphene oxide (RGO) supported Pt and Ni catalysts: seeking for economically viable biomass upgrading alternatives, Appl. Catal. A Gen. 611 (2021), https://doi.org/10.1016/j.apcata.2020.117977.

[15] D.H. Carrales-Alvarado, C. López-Olmos, A.B. Dongil, A. Kubacka, A. Guerrero-Ruiz, I. Rodríguez-Ramos, Effect of N-doping and carbon nanostructures on NiCu particles for hydrogen production from formic acid, Appl. Catal. B Environ. 298 (2021), https://doi.org/10.1016/j.apcatb.2021.120604.

[16] E. Asedegbega-Nieto, M. Perez-Cadenas, M.V. Morales, B. Bachiller-Baeza, E. Gallegos-Suarez, I. Rodriguez-Ramos, A. Guerrero-Ruiz, High nitrogen doped graphenes and their applicability as basic catalysts, Diam. Relat. Mater. 44 (2014) 26–32, https://doi.org/10.1016/j.diamond.2014.01.019.

[17] W. Jin, L. Pastor-Pérez, J.J. Villora-Pico, M.M. Pastor-Blas, A. Sepúlveda-Escribano, S. Gu, N.D. Charisiou, K. Papageridis, M.A. Goula, T.R. Reina, Catalytic conversion of palm oil to bio-hydrogenated diesel over novel N-doped activated carbon supported Pt nanoparticles, Energies 13 (2019) 1–15, https://doi.org/10.3390/en13010132.

[18] F. Barroso-Bujans, Á. Alegría, J. Colmenero, Kinetic study of the graphite oxide reduction: combined structural and gravimetric experiments under isothermal and nonisothermal conditions, J. Phys. Chem. C. 114 (2010) 21645–21651, https://doi.org/10.1021/jp108905j.

[19] Z. Lin, R. Chen, Z. Qu, J.G. Chen, Hydrodeoxygenation of biomass-derived oxygenates over metal carbides: from model surfaces to powder catalysts, Green. Chem. 20 (2018) 2679–2696, https://doi.org/10.1039/c8gc00239h.

[20] H. Shafaghat, J.M. Kim, I.G. Lee, J. Jae, S.C. Jung, Y.K. Park, Catalytic hydrodeoxygenation of crude bio-oil in supercritical methanol using supported nickel catalysts, Renew. Energy (2019), https://doi.org/10.1016/j.renene.2018.06.096.

[21] Z. Wang, X. Zhang, X. Liu, M. Lv, K. Yang, J. Meng, Co-gelation synthesis of porous graphitic carbons with high surface area and their applications, Carbon N. Y 49 (2011) 161–169, https://doi.org/10.1016/j.carbon.2010.08.056.

[22] Z.C. Yang, C.H. Tang, Y. Zhang, H. Gong, X. Li, J. Wang, Cobalt monoxide-doped porous graphitic carbon microspheres for supercapacitor application, Sci. Rep. 3 (2013) 1–7, https://doi.org/10.1038/srep02925.

[23] A.B. Dongil, L. Pastor-Pérez, A. Sepúlveda-Escribano, P. Reyes, Promoter effect of sodium in graphene-supported Ni and Ni-CeO2 catalyst for the low-temperature WGS reaction, Appl. Catal. A Gen. 505 (2015) 98–104, https://doi.org/10.1016/j.apcata.2015.07.036.

[24] R. Kumar, M. Mamlouk, K. Scott, A graphite oxide paper polymer electrolyte for direct methanol fuel cells, Int. J. Electrochem. 2011 (2011) 1–7, https://doi.org/10.4061/2011/434186.

[25] N. Wang, Z. Yang, F. Xu, K. Thummavichai, H. Chen, Y. Xia, Y. Zhu, A generic method to synthesise graphitic carbon coated nanoparticles in large scale and their derivative polymer nanocomposites, Sci. Rep. 7 (2017) 1–9, https://doi.org/10.1038/s41598-017-12200-1.

[26] G. Liu, Q. Chen, E. Oyunkhand, S. Ding, N. Yamane, G. Yang, Y. Yoneyama, N. Tsubaki, Nitrogen-rich mesoporous carbon supported iron catalyst with superior activity for Fischer-Tropsch synthesis, Carbon N. Y 130 (2018) 304–314, https://doi.org/10.1016/j.carbon.2018.01.015.

[27] X. Xu, X. Wang, Fine tuning of the sizes and phases of ZrO2 nanocrystals, Nano Res. 2 (2009) 891–902, https://doi.org/10.1007/s12274-009-9092-x.

[28] A.K. Singh, U.T. Nakate, Microwave synthesis, characterization, and photoluminescence properties of nanocrystalline zirconia, Sci. World J. (2014 () (2014), https://doi.org/10.1155/2014/349457.

[29] B. Tyagi, K. Sidhpuria, B. Shaik, R.V. Jasra, Synthesis of nanocrystalline zirconia using sol-gel and precipitation techniques, Ind. Eng. Chem. Res. 45 (2006) 8643–8650, https://doi.org/10.1021/ie060519p.

[30] M.N. Groves, C. Malardier-Jugroot, M. Jugroot, Improving platinum catalyst durability with a doped graphene support, J. Phys. Chem. C. 116 (2012) 10548–10556, https://doi.org/10.1021/jp203734d.

[31] H.S. Roh, H.S. Potdar, K.W. Jun, Carbon dioxide reforming of methane over co-precipitated Ni-CeO 2, Ni-ZrO2 and Ni-Ce-ZrO2 catalysts, Catal. Today 93–95 (2004) 39–44, https://doi.org/10.1016/j.cattod.2004.05.012.

[32] C. Zhang, W. Lv, Q. Yang, Y. Liu, Graphene supported nano particles of Pt-Ni for CO oxidation, Appl. Surf. Sci. 258 (2012) 7795–7800, https://doi.org/10.1016/j.apsusc.2012.03.131.

[33] Q. Zhang, J. Chang, T. Wang, Y. Xu, Review of biomass pyrolysis oil properties and upgrading research, Energy Convers. Manag. 48 (2007) 87–92, https://doi.org/10.1016/j.enconman.2006.05.010.